

Article

Effects of Dealumination and Desilication of Beta Zeolite on Catalytic Performance in *n*-Hexane Cracking

Yong Wang, Toshiyuki Yokoi *, Seitaro Namba and Takashi Tatsumi

Received: 11 November 2015; Accepted: 29 December 2015; Published: 5 January 2016

Academic Editor: Keith Hohn

Chemical Resources Laboratory, Tokyo Institute of Technology, 4259 Nagatsuta, Midori-ku, Yokohama 226-8503, Japan; wang.y.az@m.titech.ac.jp (Y.W.); namba@ntu.ac.jp (S.N.); ttatsumi@cat.res.titech.ac.jp (T.T.)

* Correspondence: yokoi@cat.res.titech.ac.jp; Tel.: +81-45-924-5265; Fax: +81-45-924-5238

Abstract: Catalytic cracking of *n*-hexane to selectively produce propylene on Beta zeolite was carried out. The H-Beta (HB) (Si/Al = 77) zeolite showed higher catalytic stability and propylene selectivity than the Al-rich HB (Si/Al = 12), due to its smaller number of acid sites, especially Lewis acid sites (LAS). However, catalytic stability and propylene selectivity in high *n*-hexane conversions were still not satisfactory. After dealumination with HNO₃ treatment, catalytic stability was improved and propylene selectivity during high *n*-hexane conversions was increased. On the other hand, catalytic stability was not improved after desilication with NaOH treatment, although mesopores were formed. This may be related to the partially destroyed structure. However, propylene selectivity in high *n*-hexane conversions was increased after alkali treatment. We successfully found that the catalytic stability was improved and the propylene selectivity in high *n*-hexane conversions was further increased after the NaOH treatment followed by HNO₃ treatment. This is due to the decrease in the number of acid sites and the increase in mesopores which are beneficial to the diffusion of coke precursor.

Keywords: *n*-hexane cracking; propylene; beta zeolite; dealumination; desilication; Lewis acid sites; mesopores

1. Introduction

Light alkenes, especially propylene which is mainly supplied as a by-product of ethylene production through thermal cracking of naphtha, are gaining more and more significance in the chemical industry. However, thermal cracking is an energy intensive process, where the product distribution, especially propylene/ethylene ratio, is hard to control. Therefore, catalytic cracking of naphtha has been drawing more attention [1]. Compared to the thermal steam cracking, the catalytic cracking of naphtha over acidic zeolite catalysts gives a high propylene/ethylene ratio, since the transformation of long-chain alkanes to short-chain alkenes occurs at least partly *via* the carbeniumion/ β -scission mechanism, *i.e.*, classical bimolecular cracking [2,3].

Among the zeolite catalysts examined for catalytic cracking, ZSM-5 (MFI-type) zeolite with three dimensional 10-membered ring (10-MR) channels has been recognized as a prime candidate because of its high thermal and hydrothermal stabilities and its considerable resistance to deactivation caused by coking as well as its strong acidity [4]. Yoshimura *et al.* reported that La₂O₃/P/ZSM-5 zeolite (Si/Al = 100) exhibited a high naphtha catalytic cracking activity and a high yield of *ca.* 60% to light olefins (ethylene and propylene) at 923 K, and the propylene/ethylene ratio was approximately 0.7 [1]. Recently, we carried out catalytic cracking of *n*-hexane as a model reaction of naphtha cracking over

H-ZSM-5 zeolites (Si/Al = 45) with different crystal sizes, and found that the catalytic stability could be improved by decreasing the crystal size [5]. However, the propylene selectivity at *ca.* 100% *n*-hexane conversion slightly decreased from *ca.* 32 to 26 C-% at 923 K.

To improve the propylene selectivity in catalytic cracking, zeolite catalysts with other structures have been considered. Recently, dealuminated MCM-68 (MSE-type) zeolite (Si/Al = 51) with multidimensional 10-MR or 12-MR micropores has been reported to exhibit a high propylene selectivity of *ca.* 45–50 C-% and a high durability to coke formation during *n*-hexane cracking, regardless of the reaction temperature [6]. However, the *n*-hexane conversion was only changed from *ca.* 7%–75% by changing the reaction temperature from 723 to 873 K. Thus, the selectivity to propylene was uncertain when the *n*-hexane conversion approached 100%. More recently, we reported that dealuminated MCM-22 (MWW-type) zeolite (Si/Al = 62) with two dimensional sinusoidal 10-MR channels and 12-MR supercages exhibited a high propylene selectivity of *ca.* 40 C-% with a high *n*-hexane conversion of 95% and a high catalytic stability at 923 K [7].

Beta (*BEA-type) zeolite with three dimensional 12-MR channels has been an important catalyst in the petroleum industry, especially in the alkylation process of benzene for the production of ethylbenzene and cumene [8,9]. Additionally, Beta zeolite also shows an excellent catalytic performance in FCC processes [10]. It is well-known that the Brønsted acid sites (BAS) in the zeolite catalyst act as active sites in alkane cracking, and that Lewis acid sites (LAS) can enhance the cracking reaction [11,12]. However, a large amount of acid sites, especially the LAS, would accelerate the secondary reactions of propylene and butenes and the hydride transfer, leading to coke formation followed by deactivation [7]. Thus, dealumination of zeolite catalyst leads to an increase in propylene selectivity and the improvement of catalytic stability. It was reported that dealumination of Beta zeolite occurred very easily compared to other ones such as ZSM-5 and MCM-22, due to the presence of stacking defects [13]. The dealumination of Beta zeolite by different methods such as acid treatment, steaming treatment, and chemical treatments had already been studied in the literature [14–16]. However, the effect of dealumination of Beta zeolite on the catalytic performance of alkane cracking was seldom reported [6]. More recently, we have reported that the dealuminated organic structure-directing agent (OSDA) free Beta zeolite showed a better catalytic performance in *n*-hexane cracking [17].

On the other hand, desilication proceeded by a controlled extraction of Si from the zeolite framework in alkali medium has been proven an efficient method to induce significant mesoporosity [18,19]. Recently, we found that the catalytic stability in *n*-hexane cracking can be improved by alkali treatment of ZSM-5 due to the formation of mesopores, which facilitates the diffusion of the coke precursor [20]. In addition, LAS were generated by higher concentrated NaOH treatment, leading to the increase in the selectivities to benzene, toluene and xylene (BTX) at high reaction temperatures (≥ 873 K). However, selectivity to propylene did not increase. Similarly, Bjorgen *et al.* reported that product distribution and catalytic stability in the methanol to gasoline (MTG) reaction were also altered dramatically with desilication of ZSM-5, as a result of formation of LAS [21]. Up to now, there are many reports on the effect of desilication of ZSM-5 zeolite on the catalytic performance in various reactions [20–23]. However, only a few papers on the desilication of Beta zeolite were reported [24,25]. Moreover, the effect of desilication of Beta zeolite on the catalytic performance of alkane cracking has never been reported.

In this study, the dealuminated and desilicated H-Beta zeolites (hereinafter, designated as “HB”) were prepared via acid and alkali treatment, respectively. The effects of dealumination and desilication on the physicochemical properties (including porosity and acidity) and catalytic properties (including activity, selectivity and catalytic life) of HB zeolites in the cracking of *n*-hexane as a model compound of naphtha were investigated. In addition, as a control, the physicochemical properties and catalytic properties of Al-rich HB were investigated.

2. Results and Discussion

2.1. A Summary of Catalysts' Characterization

The acid-treated HB samples were denoted as HB(77)-NT(*a* M, *b* h), where *a* and *b* were the HNO₃ concentration and treatment time, respectively. The alkali-treated HB samples were denoted as HB(77)-AT(*c* M), where *c* was the NaOH concentration. The alkali-acid-treated samples were denoted as HB(77)-AT(*c* M)-NT(*d* M), where *d* was the HNO₃ concentration.

2.1.1. XRD

Figure 1 shows the XRD patterns of the Al-rich HB(12), HB(77) and post-treated HB zeolites. Both of the HB(12) and HB(77) had a pure Beta phase and relatively high crystallinities (Figure 1A). Little change was observed in the diffractions after HNO₃ treatment, regardless of the HNO₃ concentration and treatment time (Figure 1A), meaning that the structure remained even after the acid treatment.

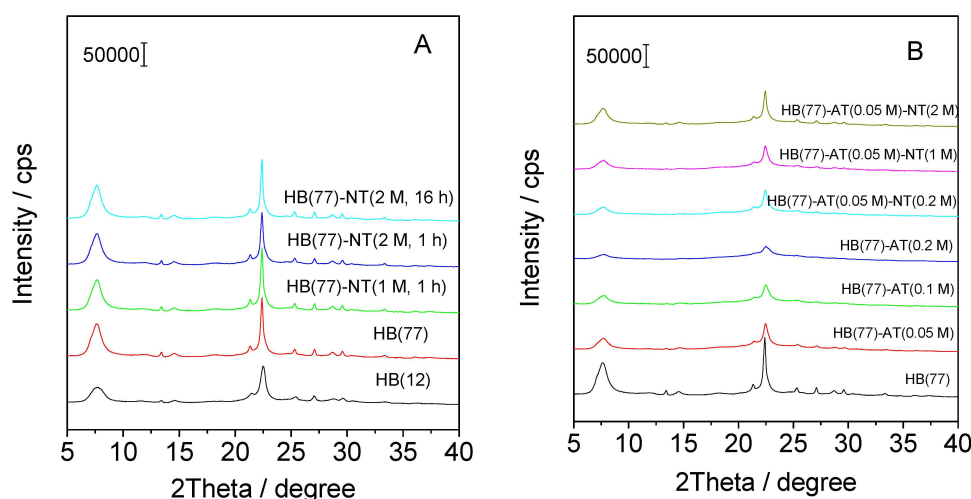


Figure 1. XRD patterns of HB(12), HB(77), acid-treated HB (A); alkali-treated and alkali-acid-treated HB (B) catalysts.

On the other hand, it was apparent that the crystallinities of the alkali-treated HB were dependent on the alkali treatment conditions, *i.e.*, NaOH concentration. The crystallinity was gradually decreased with an increase in the NaOH concentration (Figure 1B), meaning that the structure was partially destroyed due to desilication (and/or dealumination), especially after 0.2 M NaOH treatment. In addition, the crystallinity was slightly decreased after 0.05 M NaOH treatment followed by 0.2 or 1 M HNO₃ treatment. However, it was slightly recovered after 0.05 M NaOH treatment followed by 2 M HNO₃ treatment (Figure 1B).

2.1.2. SEM

The SEM images revealed that HB(12) was composed of dispersed nanoparticles with *ca.* 20 nm (Figure 2a,b). The HB(77) particles were uniform and exhibited an average particle size of *ca.* 200–300 nm (Figure 2c). At high magnification, these particles appeared to be assemblies of very small Beta zeolite crystals (*ca.* 20 nm) (Figure 2d). The morphology and size of HB particles were almost unchanged after acid treatment (Figure 2e,f). On the other hand, the edge of the aggregated HB particles became blurry and some of the large particles were broken into small ones after alkali treatment (Figure 3a–d). This may be related to the formation of amorphous species (Figure 1B). Moreover, it can be observed that some small particles formed after alkali treatment followed by acid

treatment (Figure 3e,f). These facts suggested that alkali treatment (and subsequent acid treatment) affected the particle morphology.

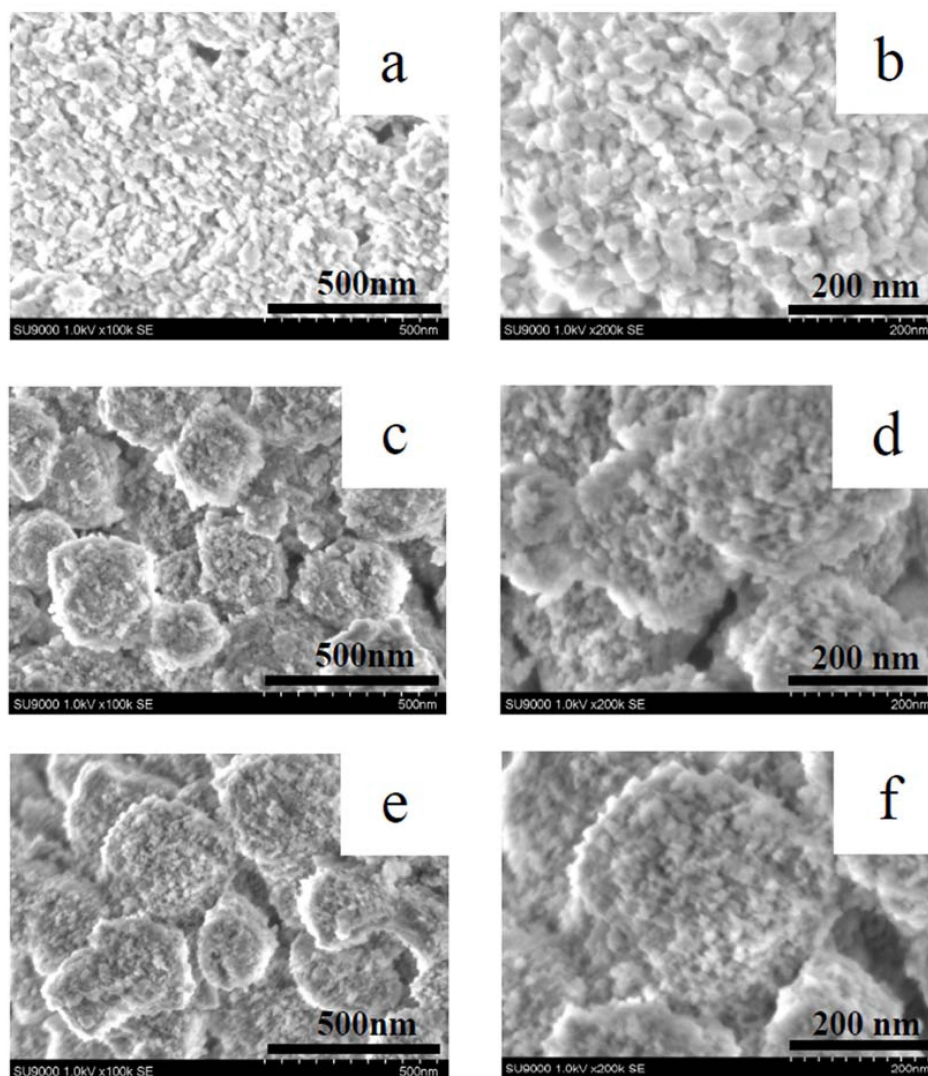


Figure 2. SEM images of HB(12) (a,b); HB(77) (c,d); and HB(77)-NT(2 M, 16 h) (e,f) catalysts.

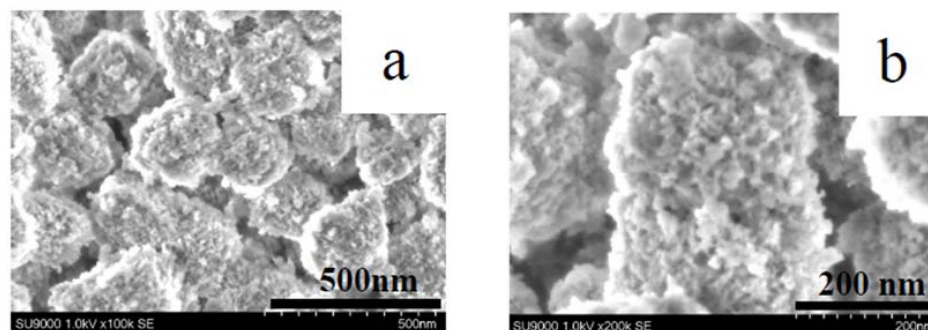


Figure 3. Cont.

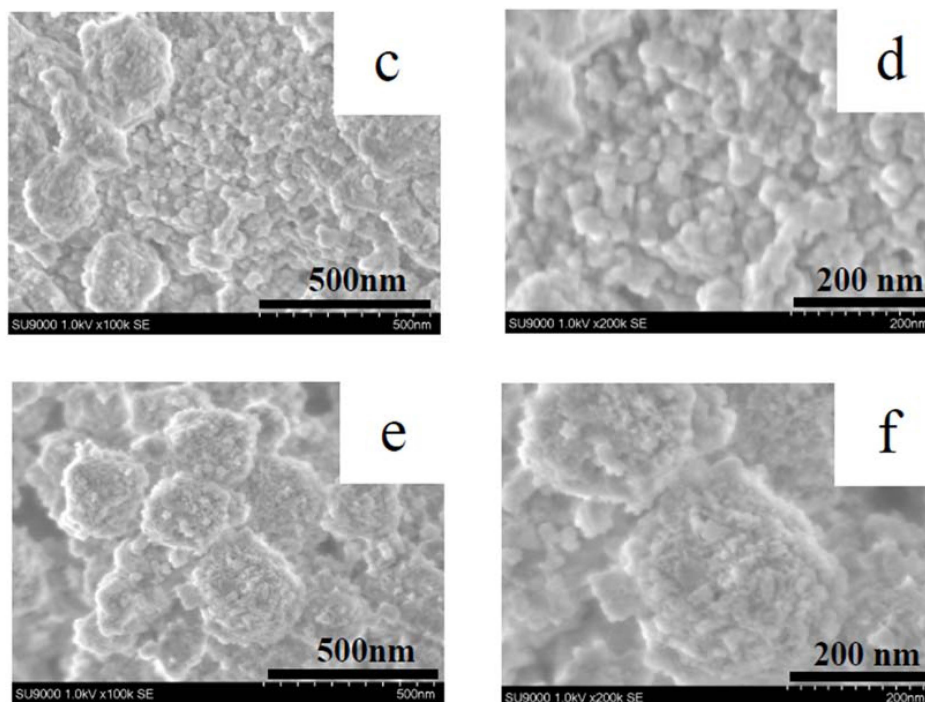


Figure 3. SEM images of HB(77)-AT(0.05 M) (a,b); HB(77)-AT(0.2 M) (c,d); and HB(77)-AT(0.05 M)-NT(1 M) (e,f) catalysts.

2.1.3. N₂ Adsorption-Desorption

Figures 4 and 5 show the N₂ adsorption-desorption isotherms and the corresponding pore size distributions of the HB(12), HB(77) and post-treated HB zeolites. Both of the HB(12) and HB(77) displayed the type I + IV isotherm, suggesting they contained a hierarchical porous system consisting of micropores and mesopores (Figure 4A). Moreover, the high N₂ adsorption at high P/P_0 (>0.9) for these two samples was attributed to the filling of the mesopores, originating from the presence of interparticle voids in the materials [26]. Correspondingly, broad peaks centered at *ca.* 4 or 3 nm in the pore size distribution patterns were observed for the HB(12) and HB(77), respectively (Figure 4B).

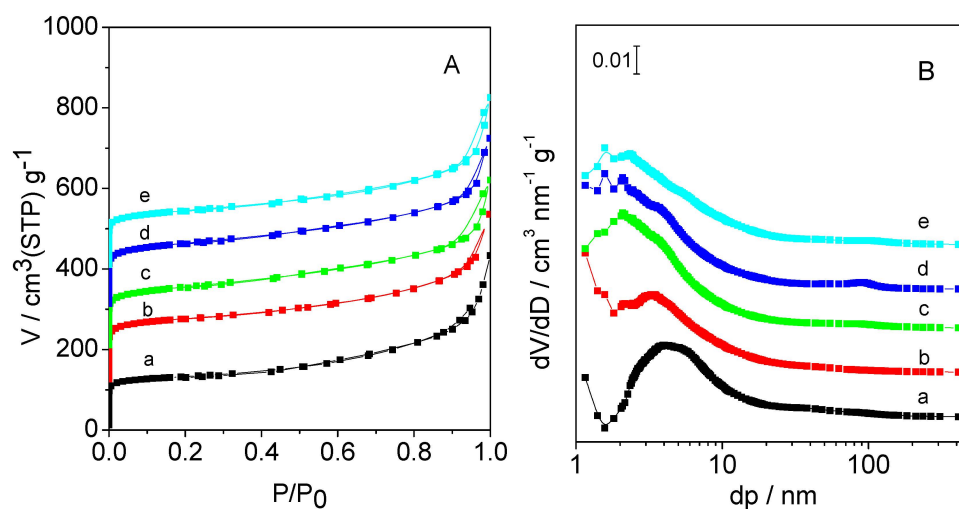


Figure 4. N₂ adsorption and desorption isotherms (A) and pore size distribution (B) of HB(12) (a); HB(77) (b); HB(77)-NT(1 M, 1 h) (c); HB(77)-NT(2 M, 1 h) (d); and HB(77)-NT(2 M, 16 h) (e) catalysts.

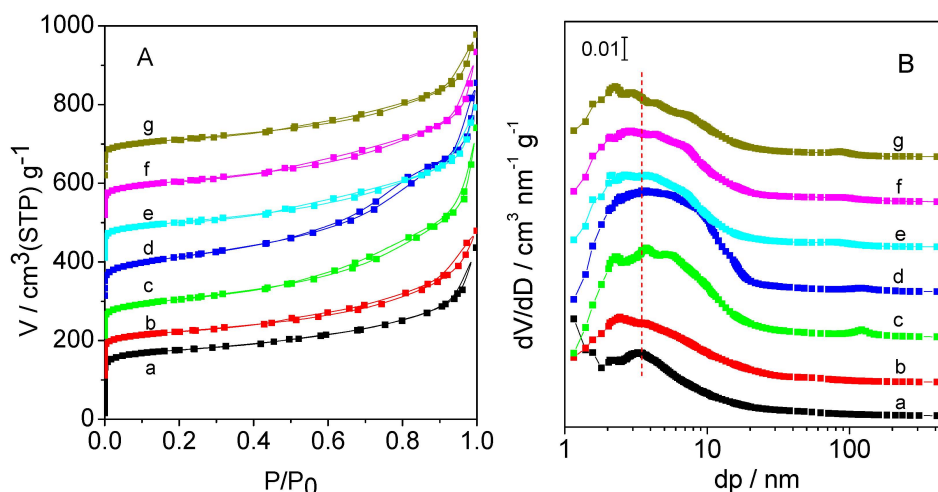


Figure 5. N_2 adsorption-desorption isotherms (A) and pore size distribution (B) of HB(77) (a); HB(77)-AT(0.05 M) (b); HB(77)-AT(0.1 M) (c); HB(77)-AT(0.2M) (d); HB(77)-AT(0.05 M)-NT(0.2 M) (e); HB(77)-AT(0.05 M)-NT(1 M) (f); and HB(77)-AT(0.05 M)-NT(2 M) (g) catalysts.

Compared to the HB(77), the acid-treated HB(77) only showed a small difference at the higher P/P_0 (>0.9), meaning that the porosity properties almost remained after HNO_3 treatment (Figure 4A). Note that the peak in the pore size distribution pattern was slightly broadened and the center of the peak was slightly shifted to the low value after the acid treatment (Figure 4B). On the other hand, the alkali-treated HB(77), especially HB(77)-AT(0.2 M), displayed a new weak hysteresis loop at P/P_0 of 0.5–0.9, indicating that new mesopores were formed by NaOH treatment (Figure 5A). Correspondingly, the peaks in the pore size distribution pattern were broadened, suggesting the presence of inhomogeneous mesopores (Figure 5B).

The isotherms of the alkali-acid-treated HB, especially HB(77)-AT(0.05 M)-NT(1 M), showed increasing step due to multilayer adsorption at P/P_0 (>0.5) and slightly enlarged hysteresis loops at P/P_0 of 0.5–0.9, indicating that the mesopores were increased by the subsequent HNO_3 treatment. A reason may be that amorphous Si and/or Al species formed by alkali treatment were partially removed by the subsequent acid treatment. Correspondingly, broad peaks centered at *ca.* 3–4 nm in the pore size distribution pattern were also observed for the alkali-acid-treated HB(77) samples (Figure 5B).

The textural properties of all HB samples obtained from N_2 adsorption isotherms are listed in Tables 1 and 2. Both of the HB(12) and HB(77) had high surface area, micropore volume and external surface area. After HNO_3 treatment, the surface area and the micropore volume of acid-treated HB(77) were slightly decreased, while the external surface area was slightly increased (Table 1).

Table 1. Physicochemical properties of HB(12), HB(77) and acid-treated HB catalysts.

Catalysts	Si/Al ^a	Acid Amount ^{b/} mmol·g ⁻¹	Textual Properties				
			S_{BET} / m ² ·g ⁻¹	S_{ext} ^d / m ² ·g ⁻¹	V_{total} ^c / cm ³ ·g ⁻¹	V_{micro} ^d / cm ³ ·g ⁻¹	V_{meso} ^e / cm ³ ·g ⁻¹
HB(12)	12	0.76	510	157	0.61	0.18	0.43
HB(77)	77	0.16	670	170	0.64	0.22	0.42
HB(77)-NT(1 M, 1 h)	80	0.16	650	176	0.63	0.20	0.43
HB(77)-NT(2 M, 1 h)	104	0.12	611	200	0.62	0.18	0.44
HB(77)-NT(2 M, 16 h)	160	0.07	590	210	0.61	0.17	0.44

^a Molar ratio determined by ICP; ^b Determined by NH_3 -TPD; ^c Total volume for pores below $p/p_0 = 0.99$;

^d Calculated by t -plot method; ^e $V_{meso} = V_{total} - V_{micro}$.

Table 2. Physicochemical properties of HB(77), alkali-treated and alkali-acid-treated catalysts.

Catalysts	Si/Al ^a	Acid Amount ^b / mmol·g ⁻¹	Textual Properties				
			S _{BET} / m ² ·g ⁻¹	S _{ext} ^d / m ² ·g ⁻¹	V _{total} ^c / cm ³ ·g ⁻¹	V _{micro} ^d / cm ³ ·g ⁻¹	V _{meso} ^e / cm ³ ·g ⁻¹
HB(77)	77	0.16	670	170	0.64	0.22	0.42
HB(77)-AT(0.05 M)	71	0.14	446	212	0.55	0.12	0.43
HB(77)-AT(0.1 M)	51	0.13	360	259	0.74	0.05	0.69
HB(77)-AT(0.2 M)	52	0.14	376	300	0.77	0.04	0.73
HB(77)-AT(0.05 M)-NT(0.2 M)	137	0.08	354	214	0.57	0.06	0.51
HB(77)-AT(0.05 M)-NT(1 M)	116	0.07	374	220	0.61	0.07	0.54
HB(77)-AT(0.05 M)-NT(2 M)	105	0.06	376	210	0.56	0.08	0.48

^a Molar ratio determined by ICP; ^b Determined by NH₃-TPD; ^c Total volume for pores below $p/p_0 = 0.99$;

^d Calculated by t -plot method; ^e $V_{meso} = V_{total} - V_{micro}$.

On the other hand, the surface area and micropore volume were decreased after the 0.05 M NaOH treatment, while the external surface area was slightly increased. Note that the total pore volume was slightly decreased, however, the mesopore volume was almost unchanged (Table 2). By increasing the NaOH concentration to 0.1 or 0.2 M, the total volume and mesopore volume increased, meaning that a large amount of mesopores were formed by these treatments. However, the surface area and micropore volume were further decreased, suggesting the severe destruction of structure (Table 2).

The surface area and micropore volume were further decreased after 0.05 M NaOH treatment followed by 0.2 M HNO₃ treatment. The possible reason for the decreases is that the framework of zeolite became unstable by alkali treatment, and it would be easily destroyed by the subsequent acid treatment. However, the total volume remained and the mesopore volume slightly increased.

2.1.4. Elemental Analysis

As shown in Table 1, the Si/Al ratio of the acid-treated HB(77) samples was gradually increased with an increase in the HNO₃ concentration or treatment time. The bulk Si/Al ratio of 160 was achieved by 2 M HNO₃ treatment for 16 h. These facts suggest that the direct acid treatment is an efficient dealumination method for Beta zeolite. This may be due to the presence of stacking defects and three dimensional 12-MR channels, which are beneficial to the removal of Al atoms from the framework and/or extra-framework [13].

On the other hand, as shown in Table 2, the Si/Al ratio was slightly decreased to 71 after 0.05 M NaOH treatment. By increasing the NaOH concentration to 0.1 or 0.2 M, the Si/Al ratio was decreased to *ca.* 50, meaning that the extraction of Si atom was more easily than Al atoms, especially during the higher concentrated NaOH treatment. Note that the Si/Al ratio was drastically increased to 137 after 0.05 M NaOH treatment followed by 0.2 M HNO₃ treatment. This result was different from the facts that the Si/Al ratio was slightly increased after the direct HNO₃ treatment (Si/Al = 80 for HB(77)-NT(1 M)). Thus, it can be concluded that the alkali treatment even under mild conditions (*i.e.*, 0.05 M NaOH treatment at room temperature for 0.5 h) would lead to the formation of many stacking defects or some mesopores which can facilitate the removal of Al atoms from the framework or extra-framework.

2.1.5. NH₃-TPD

Figures 6 and 7 show the NH₃-TPD profiles of the HB(12), HB(77) and post-treated HB samples. All these profiles were composed of two desorption peaks, the so-called “*l*-peak” and “*h*-peak”. The *l*-peak corresponds to NH₃ adsorbed on non-acidic -OH groups and on NH₄⁺, which forms by the reaction of NH₃ and Brønsted acid sites. On the other hand, the *h*-peak corresponds to NH₃ adsorbed on true acid sites [27,28]. Thus, the acid amounts were estimated by the *h*-peak areas and are listed in Tables 1 and 2.

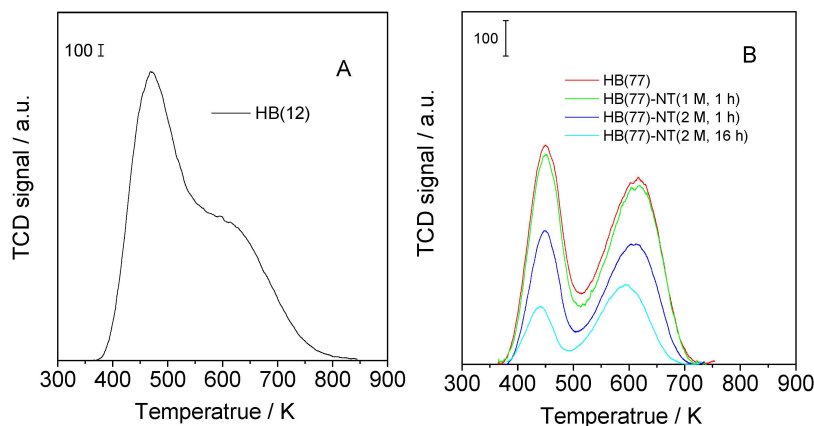


Figure 6. NH_3 -TPD profiles of HB(12) (A); HB(77) and acid-treated HB (B) catalysts.

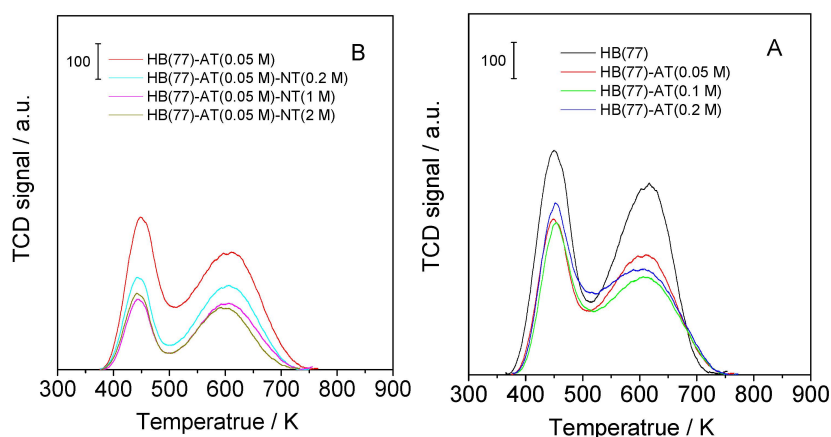


Figure 7. NH_3 -TPD profiles of HB(77), alkali-treated HB (A); and alkali-acid-treated HB (B) catalysts.

Obviously, the HB(12) had the highest acid amount among all the HB samples. In addition, the *l*-peak and *h*-peak were seriously overlapped for the HB(12), however, they can be easily separated for the HB(77) (Figure 6). This fact suggests that the HB(12) had a wider distribution of acid strength than the HB(77). As shown in Figure 6B and Table 1, the acid amount was decreased after the HNO_3 treatment, indicating dealumination occurred during the acid treatment. Moreover, the acid amount was gradually decreased along with the HNO_3 concentration or treatment time. On the other hand, as shown in Figure 7A and Table 2, the acid amount was also decreased after NaOH treatment, indicating dealumination occurred accompanied with desilication during the alkali treatment procedure. Note that the amount of acid of HB(77)-AT(0.2 M) was slightly higher than that of HB(77)-AT(0.1 M) (Figure 7A, Table 2). This may be due to the increase in the LAS generated by the higher concentrated NaOH treatment (see in Section 2.1.6). In addition, the acid amount was further decreased after 0.05 M NaOH treatment followed by HNO_3 treatment (Figure 7B, Table 2), suggesting further dealumination.

2.1.6. Pyridine Adsorption FT-IR

To clarify the acidic properties in detail, the pyridine adsorption FT-IR spectra of the HB(12), HB(77) and post-treated HB samples were measured. In the region of hydroxyl stretching vibration (Figure 8A), the HB(12) exhibited three main bands at 3781, 3741 and 3603 cm^{-1} , which are attributed to AlOH hydroxyls, isolated external silanols and structural Si(Al)OH hydroxyls, respectively [29]. The HB(77) exhibited two main bands at 3730 and 3603 cm^{-1} , which are attributed to isolated internal silanols and structural Si(Al)OH hydroxyls, respectively [29]. After HNO_3 treatment, the band at 3603 cm^{-1} decreased in intensity, however, the band at 3730 cm^{-1} increased. Additionally,

HB(77)-NT(2 M, 16 h) showed a broad band at 3700–3500 cm^{-1} ascribed to hydrogen-bonded hydroxyl groups [29]. These facts suggest that the silanols were increased by the dealumination with HNO_3 treatment. On the other hand, the band at 3603 cm^{-1} was slightly decreased in intensity after NaOH treatment (Figure 9A), indicating that the dealumination occurred accompanied by desilication during the alkali treatment. However, the band at 3741 cm^{-1} increased in intensity after NaOH treatment. The increase in the isolated external silanols was consistent with the increase in the external surface area after alkali treatment (Table 2). In addition, the band at 3603 cm^{-1} further decreased in intensity after 0.05 M NaOH treatment followed by 0.2 M HNO_3 treatment, meaning that further dealumination occurred. Note that the band at 3730 cm^{-1} decreased in intensity for HB(77)-AT(0.05 M)-NT(2 M). This may be related to the repair of the defect sites by the amorphous Si and /Al species generated by the alkali treatment in the acidic medium [30]. It can also be explained for the increases in its crystallinity, Si/Al ratio and microporous volume (Figures 1B and 5, Table 2). However, the repair of the defect sites did not increase its acid amount (Figure 7B, Table 2).

In the region of pyridine ring stretching vibration (Figures 8B and 9B), all the HB samples exhibited the bands at 1542 and 1453 cm^{-1} , which are attributed to BAS and LAS, respectively [29]. Compared to the HB(12), the HB(77) had a smaller amount of acid sites especially the LAS. After acid treatment, both of the amounts of BAS and LAS were gradually decreased with an increase in the HNO_3 concentration or treatment time. Moreover, the LAS were removed more readily than the BAS during the acid treatment [7]. Note that a new band around 1446 cm^{-1} was observed for HB(77)-NT(2 M, 16 h). This band could be the pyridine molecules coordinated with the LAS and also interaction through the H bond with the BAS, this interaction causing a shift of the corresponding bands to lower frequencies [29]. Thus, it was concluded that both acid amount and acid type of HB(77) were changed after the acid treatment.

After the NaOH treatment, the amount of BAS gradually decreased while that of the LAS gradually increased along with the NaOH concentration, indicating that dealumination occurred accompanied by desilication, and that the extra-framework Al atoms generated by the dealumination acted as the LAS. The similar results were also reported in our previous work on the desilication of ZSM-5 zeolite by alkali treatment [20]. However, the amount of LAS was drastically decreased after the subsequent HNO_3 treatment for HB(77)-AT(0.05 M), suggesting that the LAS generated by alkali treatment were easily removed [20]. Moreover, both the amount of BAS and LAS gradually decreased with an increase in HNO_3 concentration.

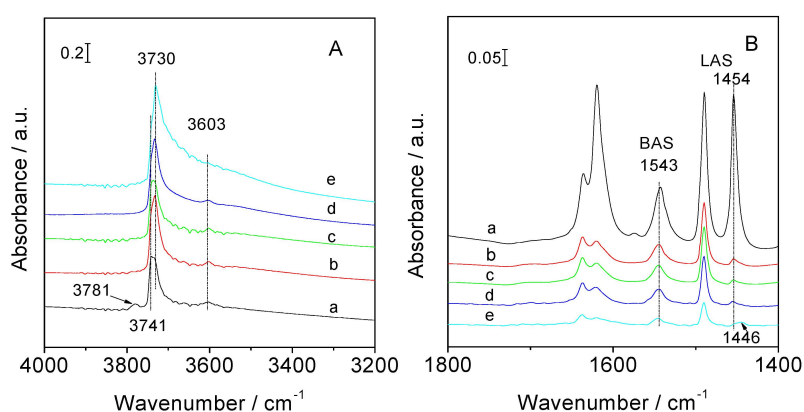


Figure 8. IR spectra of HB(12) (a); HB(77) (b); HB(77)-NT(1 M, 1 h) (c); HB(77)-NT(2 M, 1 h) (d); and HB(77)-NT(2 M, 16 h) (e) catalysts before (A) and after (B) pyridine was absorbed and then desorbed at 423 K for 1 h.

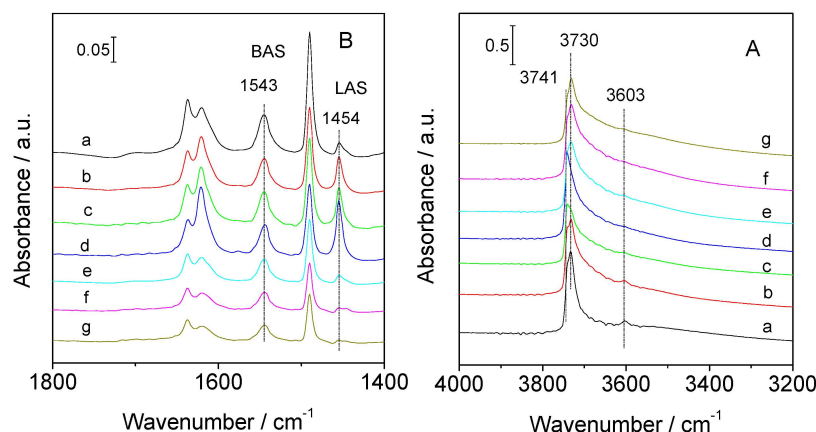


Figure 9. IR spectra of HB(77) (a); HB(77)-AT(0.05 M) (b); HB(77)-AT(0.1 M) (c); HB(77)-AT(0.2M) (d); HB(77)-AT(0.05 M)-NT(0.2 M) (e); HB(77)-AT(0.05 M)-NT(1 M) (f); and HB(77)-AT(0.05 M)-NT(2 M) (g) catalysts before (A) and after (B) pyridine was absorbed and then desorbed at 423 K for 1 h.

2.2. Catalytic Cracking of *n*-Hexane over Different HB Zeolite Catalysts

2.2.1. Al-Rich HB(12) Catalysts

Figure 10 shows the change in *n*-hexane conversion with time on stream (TOS) at different reaction temperatures for the Al-rich HB(12) catalyst. The initial *n*-hexane conversion at TOS of 15 min was increased along with the reaction temperature. At the high temperature of 923 K, the initial *n*-hexane conversion was nearly 100%; however, it sharply decreased to *ca.* 40% at TOS of 90 min. Moreover, the *n*-hexane conversion further decreased to *ca.* 23% at TOS of 210 min. This value was a little higher than that of thermal cracking under these reaction conditions [7], meaning that the catalyst was almost deactivated.

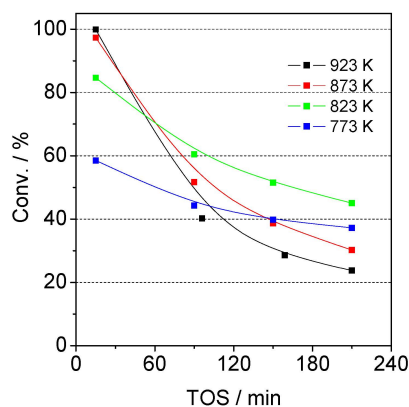


Figure 10. Change in *n*-hexane conversion with time on stream (TOS) at different reaction temperatures for HB(12) catalysts. Reaction conditions: Cat., 0.1 g; $P_{n\text{-hexane}} = 6$ kPa; $W/F_{n\text{-hexane}} = 64$ g h/mol; temp., 773–923 K.

Figure 11 shows the changes in the products selectivities at the initial stage with reaction temperature for the Al-rich HB(12) catalyst. The selectivity to propylene was almost constant at *ca.* 24 C-% in the temperature ranging between 773 and 873 K, and it was decreased to *ca.* 17 C-% at 923 K. Similarly, the selectivities to butenes were also gradually decreased along with the temperature, accompanied by a dramatic increase in the selectivities to BTX. These facts suggest that propylene and butenes are easily transformed into aromatics at high reaction temperature. The selectivities to propane and butanes were drastically decreased along with the reaction temperature, suggesting that

the subsequent reactions of propane and butanes took place at high temperatures, resulting in the formation of alkenes, BTX and so on [31]. On the other hand, the selectivity to ethylene was steeply increased along with the reaction temperature. Because ethylene is formed via primary carbenium ions [12], the apparent activation energy for the ethylene formation should be high. Thus, the higher reaction temperature must be of benefit to the ethylene formation. In addition, the selectivities to methane and ethane, which are formed solely via the monomolecular mechanism [12], were also increased along with the reaction temperature. These findings clearly indicate that the cracking via the monomolecular mechanism is more predominant at the high reaction temperature.

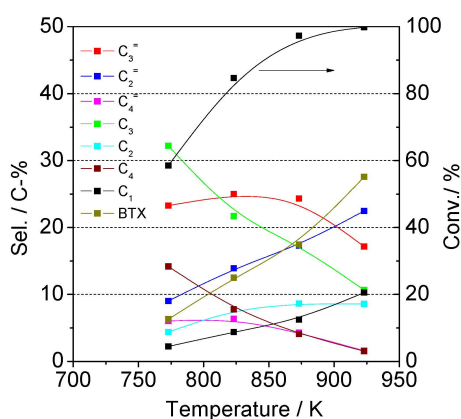


Figure 11. Effect of reaction temperature on the catalytic cracking of *n*-hexane for HB(12) catalyst. Reaction conditions: Cat., 0.1 g; $P_{n\text{-hexane}} = 6$ kPa; $W/F_{n\text{-hexane}} = 64$ g h/mol; temperature 773–923 K, TOS = 15 min. Products abbreviations: propylene (C₃⁼); ethylene (C₂⁼); butenes (C₄⁼); propane (C₃); ethane (C₂); butanes (C₄); methane (C₁); benzene, toluene and xylene (BTX).

Figure 12 shows the changes in the products' selectivities with *n*-hexane conversion for the Al-rich HB(12) catalysts at 923 K. The selectivities to propylene and butenes were drastically decreased while the selectivities to BTX were drastically increased with an increase in the *n*-hexane conversion, suggesting that BTX are formed mainly from propylene and butenes. The propylene selectivity was decreased from *ca.* 32 to 17 C-% when the *n*-hexane conversion was increased from *ca.* 88% to 100%. On the other hand, the selectivity to ethylene was increased while the selectivities to butanes were decreased with an increase in the *n*-hexane conversion. These facts suggest that ethylene would be formed not only by *n*-hexane cracking but also by butane cracking. Meanwhile, the selectivities to methane and ethane were slightly increased with an increase in the *n*-hexane conversion.

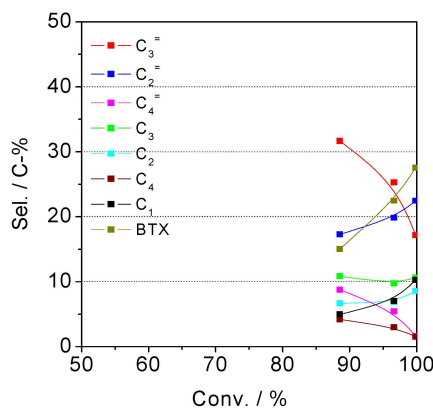


Figure 12. Change in products' selectivities with *n*-hexane conversion on HB(12) catalysts. Reaction conditions: $P_{n\text{-hexane}} = 6$ kPa; $W/F_{n\text{-hexane}} = 12.8\text{--}64$ g h/mol; temperature 923 K, TOS = 15 min. Products abbreviations: see Figure 11.

2.2.2. Comparison of HB(77) and Acid-Treated HB Catalysts

Figure 13 shows the change in *n*-hexane conversion with TOS for the HB(77) and acid-treated HB(77) catalysts at 923 K. A slight decrease in the *n*-hexane conversion from 100% at TOS of 15 min to *ca.* 95% at TOS of 90 min was observed for the HB(77). Obviously, the catalytic stability of the HB(77) was higher than that of the Al-rich HB(12) (Figure 10). However, the *n*-hexane conversion was decreased to *ca.* 73% at TOS of 210 min, and the catalytic stability was still not satisfactory. Thus, the catalytic performances of dealuminated HB zeolites with a much lower amount of acid were considered.

All the acid-treated HB(77) catalysts showed high initial *n*-hexane conversions (>97%). Compared to the HB(77), HB(77)-NT(1 M, 1 h) showed slightly higher catalytic stability. By increasing the HNO₃ concentration and treatment time, the catalytic stability was further improved. A slight decrease in *n*-hexane conversion from *ca.* 97% at TOS of 15 min to *ca.* 93% at TOS of 210 min was observed for HB(77)-NT(2 M, 16 h).

Figure 14 shows the changes in the products' selectivities with *n*-hexane conversion for the HB(77) and acid-treated HB(77) catalysts. Compared to the Al-rich HB(12) (Figure 12), the HB(77) showed a high selectivity to propylene of *ca.* 33 C-% with a *n*-hexane conversion of nearly 100% (Figure 14A), and it also showed high selectivities to butenes, butanes and propane and lower selectivities to BTX and ethylene. When the HB(77) was dealuminated by acid treatment, the selectivities to propylene and butenes at high *n*-hexane conversions were further increased, however, those to ethylene and BTX further were decreased. For example, the constant selectivity to propylene of *ca.* 46 C-% even at a high *n*-hexane conversion of *ca.* 97% was achieved for the HB(77)-NT(2 M, 16 h) (Figure 14D).

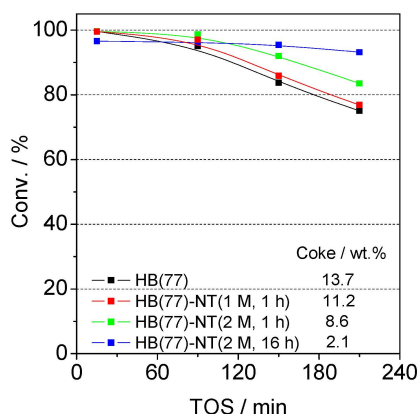


Figure 13. Change in *n*-hexane conversion with time on stream (TOS) for HB(77) and acid-treated HB catalysts. Reaction conditions: Cat., 0.1 g; $P_{n\text{-hexane}} = 6$ kPa; $W/F_{n\text{-hexane}} = 64$ g h/mol; temperature 923 K.

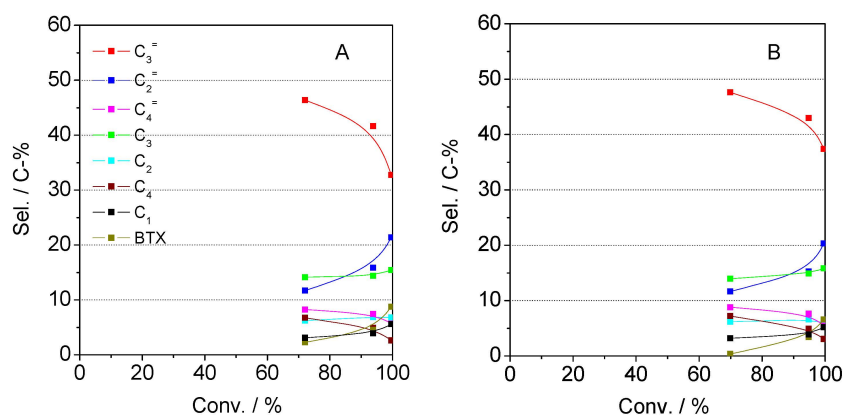


Figure 14. Cont.

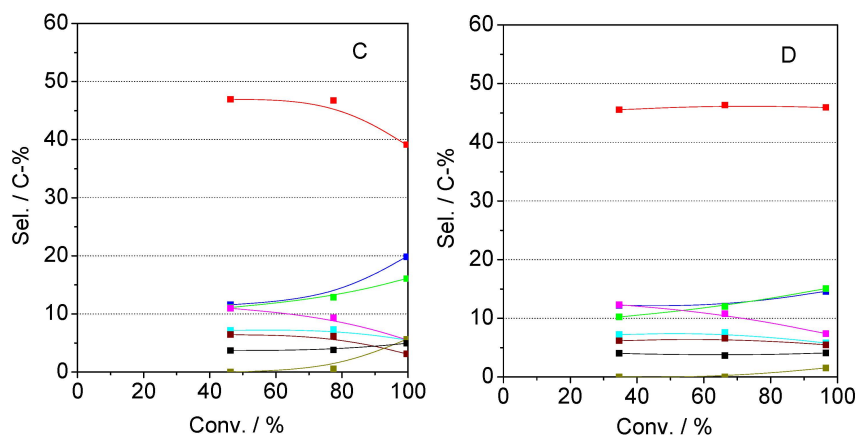


Figure 14. Changes in products' selectivities with *n*-hexane conversion on HB(77) (A); HB(77)-NT(1 M, 1 h) (B); HB(77)-NT(2 M, 1 h) (C); and HB(77)-NT(2 M, 16 h) (D) catalysts. Reaction conditions: see Figure 12. Products abbreviations: see Figure 11.

2.2.3. Comparison of HB(77), Alkali-Treated HB, and Alkali-Acid-Treated HB Catalysts

Figure 15 shows the change in *n*-hexane conversion with TOS for the HB(77), alkali-treated, and alkali-acid-treated HB(77) catalysts at 923 K. Compared to the HB(77), HB-AT(0.05 M) and HB-AT(0.1 M) still showed a nearly 100% initial *n*-hexane conversion. However, the catalytic stability was not improved after these treatments. Note that HB(77)-AT(0.2 M) showed a slightly low initial *n*-hexane conversion of *ca.* 87% and a relatively slow deactivation rate (Figure 15A). On the other hand, the catalytic stability of alkali-treated HB(77) can be improved by subsequent HNO₃ treatment, although the initial *n*-hexane conversion slightly decreased. For example, a slight decrease in *n*-hexane conversion from *ca.* 88% at TOS of 15 min to *ca.* 85% at TOS of 210 min was observed for HB-AT(0.05 M)-NT(1 M) (Figure 15B).

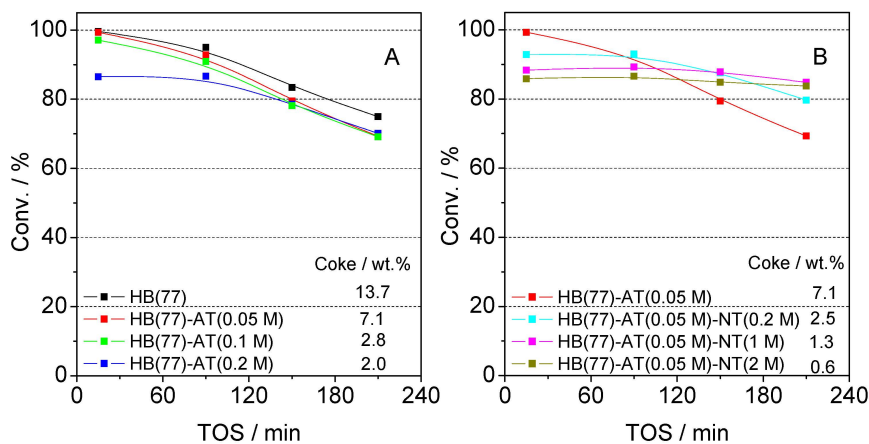


Figure 15. Change in *n*-hexane conversion with time on stream (TOS) for HB(77), alkali-treated HB (A) and alkali-acid-treated HB (B) catalysts. Reaction conditions: see Figure 13.

Figure 16 shows the changes in products' selectivities with *n*-hexane conversion for the HB(77), alkali-treated and alkali-acid-treated HB(77) catalysts. Compared to the HB(77) (Figure 16A), HB(77)-AT(0.05 M) showed a slightly higher propylene selectivity of *ca.* 36 C-% at the *n*-hexane conversion of nearly 100% (Figure 16B). Meanwhile, the HB-AT(0.05 M) also showed higher selectivities to BTX and lower selectivity to propane than the HB(77) in high *n*-hexane conversions. By increasing the NaOH concentration to 0.2 M, the selectivities to propylene and butenes in high *n*-hexane conversions

were increased while the selectivities to ethylene and propane were decreased. The HB(77)-AT(0.2 M) showed a higher selectivity to propylene of *ca.* 40 C-% even with a high *n*-hexane conversion of *ca.* 97% (Figure 16C). On the other hand, when the HB(77) was treated by 0.05 M NaOH followed by HNO₃ treatment, the selectivities to propylene and butenes in high *n*-hexane conversions drastically increased, however, those to ethylene and BTX drastically decreased. For example, the HB(77)-AT(0.05 M)-NT(1 M) showed a higher selectivity of *ca.* 48 C-% to propylene in a high *n*-hexane conversion of *ca.* 90% (Figure 16D).

In summary, the HB(77) with a lower amount of acid showed higher selectivity to propylene with high *n*-hexane conversions and a higher catalytic stability at a high reaction temperature than the Al-rich HB(12). The catalytic performance of HB(77) including propylene selectivity and catalytic stability can be further improved by acid treatment. On the other hand, selectivity to propylene in high *n*-hexane conversions can also be improved by alkali treatment; however, catalytic stability cannot be improved. Furthermore, both selectivity to propylene in high *n*-hexane conversions and catalytic stability can be improved after alkali treatment followed by acid treatment, although the initial *n*-hexane conversion was slightly decreased.

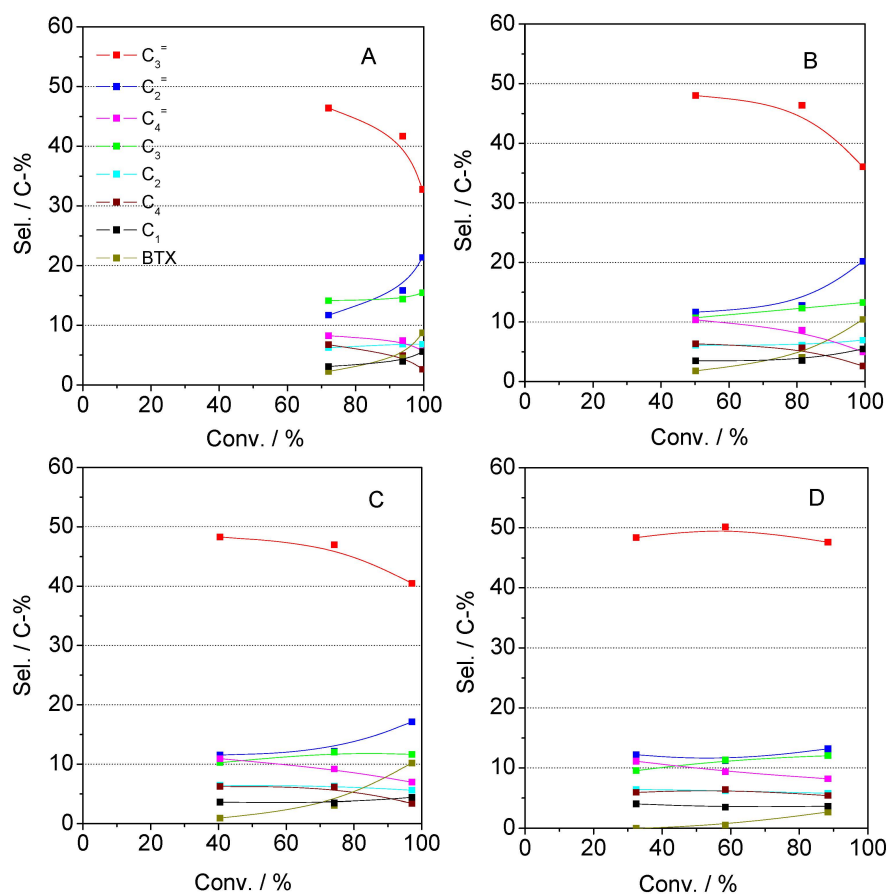


Figure 16. Changes in products' selectivities with *n*-hexane conversion on HB(77) (A); HB(77)-AT(0.05 M) (B); HB(77)-AT(0.2 M) (C); and HB(77)-AT(0.05 M)-NT(1 M) (D) catalysts. Reaction conditions: see Figure 12. Products abbreviations: see Figure 11.

2.3. Effect of Dealumination and Desilication on the Catalytic Performance

In this section, catalytic properties, especially catalytic stability and propylene selectivity in high *n*-hexane conversions for different HB catalysts, were related to their physicochemical properties (including porosity and acidity), and the effects of dealumination and desilication on their catalytic performances in *n*-hexane cracking were discussed.

2.3.1. Effect of Dealumination

As shown in Figures 10–12 Al-rich HB(12) showed a poor catalytic stability, a low propylene selectivity and a high BTX selectivity at the high temperature of 923 K. The inferior catalytic performance can be explained by two possible reasons. One reason may be related to the large amount of acid sites (Table 1), which would accelerate the secondary reactions of propylene and butenes and the hydride transfer, leading to a large amount of coke being formed (163 mg/g-catalyst at TOS of 210 min). The other reason may be related to the special structure of Beta zeolite. The polymerization of olefins and the successive formation of coke components may predominantly occur in the three dimensional 12-MR micropores and their wide intersections [6]. Note that the HB(12) composed of nanoparticles had a higher external surface area and mesopore volume (Figure 2, Table 1) which are beneficial to the products' diffusion. Therefore, we concluded that the poor catalytic performance of HB(12) was mainly related to its acidic properties.

Compared to Al-rich HB(12), HB(77) showed high selectivities to propylene and butenes, however, low selectivities to BTX, ethylene, propane and butanes (Figures 13 and 14A) were demonstrated. It could be due to the smaller amount of acid sites, especially the LAS (Table 1, Figures 6 and 8B). Note that, although the HB(77) had superior catalytic stability, the amount of coke formed on the HB(77) (137 mg/g-catalyst at TOS of 210 min) was comparable to that of Al-rich HB(12).

As shown in Figures 13 and 14 catalytic stability and propylene selectivity with high *n*-hexane conversions can be greatly improved by dealumination with acid treatment. Note that crystal morphology and size were almost unchanged and the textural properties remained after the acid treatment (Figure 2, Table 1). The improvement in catalytic performance would be due to a further decrease in the amount of acid sites, especially the LAS (Table 1, Figures 6B and 8B), resulting in suppression of the hydride transfer and coke formation (e.g., 21 mg/g-catalyst at TOS of 210 min for HB(77)-NT(2 M, 16 h)). This conclusion was consistent with our previous work on *n*-hexane cracking over dealuminated H-MCM-22 zeolites [7].

2.3.2. Effect of Desilication

As shown in Figure 15A, catalytic stability was not improved after 0.05 or 0.1 M NaOH treatment; however, it was slightly improved after 0.2 M NaOH treatment, although the initial *n*-hexane conversion was slightly decreased. This may be related to the partially destroyed structure (Figures 1B and 5, Table 2). On the other hand, the catalytic stability was remarkably improved after 0.05 M NaOH treatment followed by HNO₃ treatment, although the initial *n*-hexane conversion was slightly decreased (Figure 15B). This may be due to the decrease in the number of acid sites (Table 2, Figure 9), leading to a smaller amount of coke being formed (e.g., 13 mg/g-catalyst at TOS of 210 min for HB(77)-AT(0.05 M)-NT(1 M)). In addition, the increase in the mesopores formed by the subsequent acid treatment would be beneficial to the diffusion of coke precursor (Table 2).

As to the products' distribution, the propylene selectivity was slightly increased after 0.05 M NaOH treatment. Meanwhile, the BTX selectivities were increased while the propane selectivity was decreased (Figure 16B). This fact suggested that the dehydrogenation of propane and subsequent aromatization of olefins were improved by 0.05 M NaOH treatment, due to the increase in the amount of LAS (Figure 9B). Similar results were observed in our work on *n*-hexane cracking over alkali-treated H-ZSM-5 zeolites [20]. By increasing the NaOH concentration to 0.2 M, the propane selectivity was further decreased. This is due to the further increase in the amount of LAS which accelerated the dehydrogenation of propane. However, the BTX selectivities remained, and the selectivities to propylene and butenes increased while the selectivity to ethylene decreased. It can be explained by two possible reasons. One possible reason would be related to the decrease in the amount of BAS (Figure 9B), which suppressed the secondary reactions of propylene and butenes. Another possible reason may be due to the strong increase in the mesopores after 0.2 M NaOH treatment (Table 2, Figure 5), which was beneficial to the diffusion of the formed olefins and the resultant lower amount of coke being formed (20 mg/g-catalyst at TOS of 210 min). This finding differed from our previous

results on *n*-hexane cracking over alkali-treated H-ZSM-5 zeolites, in which the amount of coke used for alkali-treated catalyst was larger than that for the untreated one [20].

On the other hand, the selectivities to propylene and butenes in high *n*-hexane conversions were remarkably increased; however, those to ethylene and BTX were drastically decreased after 0.05 M NaOH treatment followed by acid treatment. These findings indicated that the secondary reactions to form BTX from propylene and butenes and the subsequent cracking reaction of butanes and/or propane to form ethylene could be further suppressed, due to the dramatic decrease in the number of acid sites, especially the LAS (Table 2, Figure 9). In addition, another possible reason would be related to the increase in the mesopores during the subsequent acid treatment (Table 2, Figure 5), which was beneficial to the diffusion of the formed olefins.

3. Experimental Section

3.1. Catalyst Preparation

3.1.1. Dealumination of H-Beta

The H-Beta (Si/Al = 12) and H-Beta (Si/Al = 77) zeolites, denoted as HB(12) and HB(77), were supplied from the Catalysis Society of Japan and Sud-Chemie AG, Munchen, Germany, respectively. The HB(77) was used as the parent material and dealuminated by acid treatment. Specifically, 1 g HB(77) was suspended and stirred in a 1–2 M HNO₃ (60%, Wako, Osaka, Japan) solution at 393 K for 1 or 16 h. The weight ratio of solid to liquid ratio was 1:30. The acid-treated HB samples were denoted as HB(77)-NT(*a* M, *b* h), where *a* and *b* were the HNO₃ concentration and treatment time, respectively.

3.1.2. Desilication of H-Beta

The HB(77) zeolite was used as the parent material and desilicated by alkali treatment. Specifically, 1 g HB(77) was suspended and stirred in a 0.05–0.2 M NaOH (97%, Wako, Osaka, Japan) solution at room temperature for 0.5 h. The weight ratio of solid to liquid ratio was 1:30. The samples were filtered, washed, and dried at 373 K and then converted to the H-type ones with 1 M NH₄NO₃ (99%, Wako, Osaka, Japan) twice at 353 K for 2 h, followed by calcination in air at 773 K for 2 h. The alkali-treated HB samples were denoted as HB(77)-AT(*c* M), where *c* was the NaOH concentration. On the other hand, the alkali-treated HB sample was further dealuminated by acid treatment. Specifically, 1 g HB(77)-AT(0.05 M) was suspended and stirred in a 0.2–2 M HNO₃ solution at 393 K for 1 h. The weight ratio of solid to liquid ratio was 1:30. Thus obtained samples were filtered, washed, and dried at 373 K. The samples were denoted as HB(77)-AT(*c* M)-NT (*d* M), where *d* was the HNO₃ concentration.

3.2. Catalyst Characterization

The catalysts were characterized by various techniques. The Si/Al ratio was determined by inductively coupled plasma-atomic emission spectrometer (ICP-AES) on a Shimadzu ICPE-9000 (Shimadzu, Kyoto, Japan). The X-ray diffraction (XRD) patterns were recorded on a Rint-Ultima III (Rigaku, Tokyo, Japan) using a Cu K α X-ray source. The N₂ adsorption was carried out at 77 K on a Belsorp-mini II (BEL, Osaka, Japan). The crystal morphology and size were measured by field emission scanning electron microscopy (FE-SEM) on a Hitachi SU-9000 microscope (Hitachi, Tokyo, Japan). Thermogravimetric analyses (TGA) were conducted on a Rigaku Thermo plus EVO II equipment (Rigaku, Tokyo, Japan) in air atmosphere.

Temperature-programmed desorption of ammonia (NH₃-TPD) profiles were recorded on a BEL Multitrack TPD equipment (BEL, Osaka, Japan). IR spectra were collected on a Jasco FT/IR-6100 spectrometer (Jasco, Tokyo, Japan) equipped with a TGS detector. The IR spectra of adsorbed pyridine were recorded as follows: a self-supported wafer (9.6 mg·cm⁻² thickness and 2 cm diameter) was set in a quartz IR cell sealed with CaF₂ windows, where it was evacuated at 723 K for 2 h before pyridine adsorption. The adsorption was carried out by exposing the wafer to pyridine vapor (1.3 kPa) at 423 K

for 0.5 h. Physisorbed pyridine was removed by evacuation at 423 K for 1 h. IR spectra were collected at 423 K.

3.3. Catalytic Cracking of *n*-Hexane

The catalytic cracking of *n*-hexane was carried out with a fixed-bed flow reactor under atmospheric pressure. Typically, 0.1 g of catalyst (18–30 mesh size) was put into a quartz tubular reactor (6 mm inner diameter) and activated in a dry air flow of 20 mL·min⁻¹ at 923 K for 1 h. The height of catalyst bed was *ca.* 1 cm. The temperature was measured by a thermocouple in the top of the catalyst bed. After the reactor temperature was adjusted to the desired one, *n*-hexane vapor diluted in the helium was fed into the reactor. The initial partial pressure of *n*-hexane was set at 6 kPa. To investigate the effect of contact time on *n*-hexane catalytic cracking, the catalyst weight to the *n*-hexane flow rate ratio ($W/F_{n\text{-hexane}}$) was varied from 12.8 to 64 g h/mol.

The reaction products were analyzed with an on-line gas chromatography (GC-14B, Shimadzu, Kyoto, Japan) with an FID detector and a HP-AL/S column (30 m × 0.535 mm × 15 μm). The *n*-hexane conversion was calculated based on the peak area in the GC spectra before and after reaction. The selectivities to hydrocarbon products represent the products' distribution and were calculated using area normalization method. Because hydrocarbons generally have molar response factors that are equal to number of carbon atoms in their molecule when using FID, the relative correction factors for different hydrocarbons are approximately 1.0 based on the carbon numbers. Coke amount was calculated by thermogravimetry analysis (TGA). The weight loss from 673 to 1073 K in each TG profile was defined as the contents of coke in the used catalyst.

4. Conclusions

HB(77) exhibited higher catalytic stability and propylene selectivity than Al-rich HB(12), due to its smaller number of acid sites, especially the LAS. Dealumination of HB(77) by acid treatment improved catalytic stability and increased propylene selectivity in high *n*-hexane conversions. This may be attributed to the decrease in the number of acid sites, especially the LAS which accelerate the secondary reactions of propylene and butenes, the hydride transfer, and the resultant coke formation.

On the other hand, the desilication of HB(77) by alkali treatment did not improve catalytic stability, although mesopores were formed. This may be related to the partially destroyed structure. However, alkali treatment increased propylene selectivity in high *n*-hexane conversions. Furthermore, alkali treatment followed by acid treatment improved catalytic stability and increased propylene selectivity in high *n*-hexane conversions. This may be due to the decrease in the number of acid sites and the increase in mesopores which are beneficial to the diffusion of coke precursor.

Acknowledgments: This work was supported by the green sustainable chemistry project of New Energy and Industrial Technology Development Organization (NEDO).

Author Contributions: The present work was conducted under the supervision of Seitaro Namba and Takashi Tatsumi. Toshiyuki Yokoi did the main research consulting and paper editing, and is named the correspondent author of the submitted work. Yong Wang did the experimental work and paper writing.

Conflicts of Interest: The authors declare no conflict of interest.

References

1. Yoshimura, Y.; Kijima, N.; Hayakawa, T.; Murata, K.; Suzuki, K.; Mizukami, F.; Matano, K.; Konishi, T.; Oikawa, T.; Saito, M.; *et al.* Catalytic cracking of naphtha to light olefins. *Catal. Surv. Jpn.* **2000**, *4*, 157–167. [[CrossRef](#)]
2. Wojciechowski, B.W. The reaction mechanism of catalytic cracking: quantifying activity, selectivity, and catalyst decay. *Catal. Rev. Sci. Eng.* **1998**, *40*, 209–328. [[CrossRef](#)]
3. Kissin, Y.V. Chemical mechanism of catalytic cracking over solid acidic catalysts: Alkanes and alkenes. *Catal. Rev. Sci. Eng.* **2001**, *43*, 85–146. [[CrossRef](#)]

4. Rahimi, N.; Karimzadeh, R. Catalytic cracking of hydrocarbons over modified ZSM-5 zeolites to produce light olefins: A review. *Appl. Catal. A* **2011**, *398*, 1–17. [[CrossRef](#)]
5. Mochizuki, H.; Yokoi, T.; Imai, H.; Watanabe, R.; Namba, S.; Kondo, J.N.; Tatsumi, T. Facile control of crystallite size of ZSM-5 catalyst for cracking of hexane. *Microporous Mesoporous Mater.* **2011**, *145*, 165–171. [[CrossRef](#)]
6. Inagaki, S.; Takechi, K.; Kubota, Y. Selective formation of propylene by hexane cracking over MCM-68 zeolite catalyst. *Chem. Commun.* **2010**, *46*, 2662–2664. [[CrossRef](#)]
7. Wang, Y.; Yokoi, T.; Namba, S.; Kondo, J.N.; Tatsumi, T. Catalytic cracking of *n*-hexane for producing propylene on MCM-22 zeolites. *Appl. Catal. A* **2015**, *504*, 192–202. [[CrossRef](#)]
8. Bellussi, G.; Pazzuconi, G.; Perego, C.; Girotti, G.; Terzoni, G. Liquid-phase alkylation of benzene with light olefins catalyzed by β -zeolites. *J. Catal.* **1995**, *157*, 227–234. [[CrossRef](#)]
9. Wichterlová, B.; Čejka, J.; Žilková, N. Selective synthesis of cumene and *p*-cymene over Al and Fe silicates with large and medium pore structures. *Microporous Mater.* **1996**, *6*, 405–414. [[CrossRef](#)]
10. Corma, A.; González-Alfaro, V.; Orchillés, A.V. The role of pore topology on the behaviour of FCC zeolite additives. *Appl. Catal. A* **1999**, *187*, 245–254. [[CrossRef](#)]
11. Haag, W.O.; Lago, R.M.; Weisz, P.B. The active site of acidic aluminosilicate catalysts. *Nature* **1984**, *309*, 589–591. [[CrossRef](#)]
12. Corma, A.; Orchillés, A.V. Current views on the mechanism of catalytic cracking. *Microporous Mesoporous Mater.* **2000**, *35–36*, 21–30. [[CrossRef](#)]
13. Müller, M.; Harvey, G.; Prins, R. Comparison of the dealumination of zeolites beta, mordenite, ZSM-5 and ferrierite by thermal treatment, leaching with oxalic acid and treatment with SiCl_4 by ^1H , ^{29}Si and ^{27}Al MAS NMR. *Microporous Mesoporous* **2000**, *34*, 135–147. [[CrossRef](#)]
14. Baran, R.; Millot, Y.; Onfroy, T.; Krafft, J.M.; Dzwigaj, S. Influence of the nitric acid treatment on Al removal, framework composition and acidity of BEA zeolite investigated by XRD, FTIR and NMR. *Microporous Mesoporous Mater.* **2012**, *163*, 122–130. [[CrossRef](#)]
15. Maier, S.M.; Jentys, A.; Lercher, J.A. Steaming of zeolite BEA and its effect on acidity: A comparative NMR and IR spectroscopic study. *J. Phys. Chem. C* **2011**, *115*, 8005–8013. [[CrossRef](#)]
16. Parker, W.O.; Angelis, A.; Flego, C.; Millini, R.; Perego, C.; Zanardi, S. Unexpected destructive dealumination of zeolite Beta by silylation. *J. Phys. Chem. C* **2010**, *114*, 8459–8468. [[CrossRef](#)]
17. Wang, Y.; Otomo, R.; Tatsumi, T.; Yokoi, T. Dealumination of organic structure-directing agent (OSDA) free betazeolite for enhancing its catalytic performance in *n*-hexane cracking. *Microporous Mesoporous Mater.* **2016**, *220*, 275–281. [[CrossRef](#)]
18. Ogura, M.; Shinomiya, S.Y.; Tateno, J.; Nara, Y.; Nomura, M.; Kikuchi, E.; Matsukata, M. Alkali-treatment technique-new method for modification of structural and acid-catalytic properties of ZSM-5 zeolites. *Appl. Catal. A* **2001**, *219*, 33–43. [[CrossRef](#)]
19. Groen, J.C.; Moulijn, J.A.; Pérez-Ramirez, J. Desilication: On the controlled generation of mesoporosity in MFI zeolites. *J. Mater. Chem.* **2006**, *16*, 2121–2131.
20. Mochizuki, H.; Yokoi, T.; Imai, H.; Namba, S.; Kondo, J.N.; Tatsumi, T. Effect of desilication of H-ZSM-5 by alkali treatment on catalytic performance in hexane cracking. *Appl. Catal. A* **2012**, *449*, 188–197. [[CrossRef](#)]
21. Bjørgen, M.; Joensen, F.; Holm, M.S.; Olsbye, U.; Lillerud, K.P.; Svelle, S. Methanol to gasoline over zeolite H-ZSM-5: Improved catalyst performance by treatment with NaOH. *Appl. Catal. A* **2008**, *345*, 43–50. [[CrossRef](#)]
22. Jung, J.S.; Park, J.W.; Seo, G. Catalytic cracking of *n*-octane over alkali-treated MFI zeolites. *Appl. Catal. A* **2005**, *288*, 149–157. [[CrossRef](#)]
23. Schmidt, F.; Lohe, M.R.; Büchner, B.; Giordanino, F.; Bonino, F.; Kaskel, S. Improved catalytic performance of hierarchical ZSM-5 synthesized by desilication with surfactants. *Microporous Mesoporous Mater.* **2013**, *165*, 148–157. [[CrossRef](#)]
24. Groen, J.C.; Peffer, L.A.A.; Moulijn, J.A.; Pérez-Ramirez, J. On the introduction of intracrystalline mesoporosity in zeolites upon desilication in alkaline medium. *Microporous Mesoporous Mater.* **2004**, *69*, 29–34. [[CrossRef](#)]
25. Wu, Y.H.; Tian, F.P.; Liu, J.; Song, D.; Jia, C.Y.; Chen, Y.Y. Enhanced catalytic isomerization of α -pinene over mesoporous zeolite beta of low Si/Al ratio by NaOH treatment. *Microporous Mesoporous Mater.* **2012**, *162*, 168–174. [[CrossRef](#)]

26. Cambor, M.A.; Corma, A.; Valencia, S. Characterization of nanocrystalline zeolite Beta. *Microporous Mesoporous Mater.* **1998**, *25*, 59–74. [[CrossRef](#)]
27. Niwa, M.; Iwamoto, M.; Segawa, K. Temperature-Programmed Desorption of Ammonia on Zeolites. Influence of the experimental conditions on the acidity measurement. *Bull. Chem. Soc. Jpn.* **1986**, *59*, 3735–3739. [[CrossRef](#)]
28. Katada, N.; Igi, H.; Kim, J.H.; Niwa, M. Determination of the acidic properties of zeolite by theoretical analysis of Temperature-Programmed Desorption of ammonia based on adsorption equilibrium. *J. Phys. Chem. B* **1997**, *101*, 5969–5977. [[CrossRef](#)]
29. Marques, J.P.; Gener, I.; Ayrault, P.; Bordado, J.C.; Lopes, J.M.; Ribeiro, F.R.; Guisnet, M. Infrared spectroscopic study of the acid properties of dealuminated BEA zeolites. *Microporous Mesoporous Mater.* **2003**, *60*, 251–262. [[CrossRef](#)]
30. Oumi, Y.; Mizuno, R.; Azuma, K.; Nawata, S.; Fukushima, T.; Uozumi, T.; Sano, T. Reversibility of dealumination-realumination process of BEA zeolite. *Appl. Catal. A* **2001**, *49*, 103–109. [[CrossRef](#)]
31. Jiang, G.Y.; Zhang, L.; Zhao, Z.; Zhou, X.Y.; Duan, A.J.; Xu, C.M.; Gao, J.S. Highly effective P-modified HZSM-5 catalyst for the cracking of C₄ alkanes to produce light olefins. *Appl. Catal. A* **2008**, *340*, 176–182. [[CrossRef](#)]



© 2016 by the authors; licensee MDPI, Basel, Switzerland. This article is an open access article distributed under the terms and conditions of the Creative Commons by Attribution (CC-BY) license (<http://creativecommons.org/licenses/by/4.0/>).